

Search for $\eta_1(1855)$ in $\chi_{cJ} \rightarrow \eta\eta\eta'$ decays

M. Ablikim¹, M. N. Achasov^{4,c}, P. Adlarson⁷⁷, X. C. Ai⁸², R. Aliberti³⁶, A. Amoroso^{76A,76C}, Q. An^{73,59,a}, Y. Bai⁵⁸, O. Bakina³⁷, Y. Ban^{47,h}, H.-R. Bao⁶⁵, V. Batozskaya^{1,45}, K. Begzsuren³³, N. Berger³⁶, M. Berlowski⁴⁵, M. Bertani^{29A}, D. Betttoni^{30A}, F. Bianchi^{76A,76C}, E. Bianco^{76A,76C}, A. Bortone^{76A,76C}, I. Boyko³⁷, R. A. Briere⁵, A. Brueggemann⁷⁰, H. Cai⁷⁸, M. H. Cai^{39,k,l}, X. Cai^{1,59}, A. Calcaterra^{29A}, G. F. Cao^{1,65}, N. Cao^{1,65}, S. A. Cetin^{63A}, X. Y. Chai^{47,h}, J. F. Chang^{1,59}, G. R. Che⁴⁴, Y. Z. Che^{1,59,65}, C. H. Chen⁹, Chao Chen⁵⁶, G. Chen¹, H. S. Chen^{1,65}, H. Y. Chen²¹, M. L. Chen^{1,59,65}, S. J. Chen⁴³, S. L. Chen⁴⁶, S. M. Chen⁶², T. Chen^{1,65}, X. R. Chen^{32,65}, X. T. Chen^{1,65}, X. Y. Chen^{12,g}, Y. B. Chen^{1,59}, Y. Q. Chen¹⁶, Y. Q. Chen³⁵, Z. Chen²⁵, Z. J. Chen^{26,i}, Z. K. Chen⁶⁰, S. K. Choi¹⁰, X. Chu^{12,g}, G. Cibinetto^{30A}, F. Cossi^{76C}, J. Cottet-Meldrum⁶⁴, J. J. Cui⁵¹, H. L. Dai^{1,59}, J. P. Dai⁸⁰, A. Dbeysi¹⁹, R. E. de Boer³, D. Dedovich³⁷, C. Q. Deng⁷⁴, Z. Y. Deng¹, A. Denig³⁶, I. Denysenko³⁷, M. Destefanis^{76A,76C}, F. De Mori^{76A,76C}, B. Ding^{68,1}, X. X. Ding^{47,h}, Y. Ding⁴¹, Y. Ding³⁵, Y. X. Ding³¹, J. Dong^{1,59}, L. Y. Dong^{1,65}, M. Y. Dong^{1,59,65}, X. Dong⁷⁸, M. C. Du¹, S. X. Du^{12,g}, S. X. Du⁸², Y. Y. Duan⁵⁶, P. Egorov^{37,b}, G. F. Fan⁴³, J. J. Fan²⁰, Y. H. Fan⁴⁶, J. Fang⁶⁰, J. Fang^{1,59}, S. S. Fang^{1,65}, W. X. Fang¹, Y. Q. Fang^{1,59}, R. Farinelli^{30A}, L. Fava^{76B,76C}, F. Feldbauer³, G. Felici^{29A}, C. Q. Feng^{73,59}, J. H. Feng¹⁶, L. Feng^{39,k,l}, Q. X. Feng^{39,k,l}, Y. T. Feng^{73,59}, M. Fritsch³, C. D. Fu¹, J. L. Fu⁶⁵, Y. W. Fu^{1,65}, H. Gao⁶⁵, X. B. Gao⁴², Y. Gao^{73,59}, Y. N. Gao^{47,h}, Y. N. Gao²⁰, Y. Y. Gao³¹, S. Garbolino^{76C}, I. Garzia^{30A,30B}, P. T. Ge²⁰, Z. W. Ge⁴³, C. Geng⁶⁰, E. M. Gersabeck⁶⁹, A. Gilman⁷¹, K. Goetzen¹³, J. D. Gong³⁵, L. Gong⁴¹, W. X. Gong^{1,59}, W. Gradl³⁶, S. Gramigna^{30A,30B}, M. Greco^{76A,76C}, M. H. Gu^{1,59}, Y. T. Gu¹⁵, C. Y. Guan^{1,65}, A. Q. Guo³², L. B. Guo⁴², M. J. Guo⁵¹, R. P. Guo⁵⁰, Y. P. Guo^{12,g}, A. Guskov^{37,b}, J. Gutierrez²⁸, K. L. Han⁶⁵, T. T. Han¹, F. Hanisch³, K. D. Hao^{73,59}, X. Q. Hao²⁰, F. A. Harris⁶⁷, K. K. He⁵⁶, K. L. He^{1,65}, F. H. Heinsius³, C. H. Heinz³⁶, Y. K. Heng^{1,59,65}, C. Herold⁶¹, P. C. Hong³⁵, G. Y. Hou^{1,65}, X. T. Hou^{1,65}, Y. R. Hou⁶⁵, Z. L. Hou¹, H. M. Hu^{1,65}, J. F. Hu^{57,j}, Q. P. Hu^{73,59}, S. L. Hu^{12,g}, T. Hu^{1,59,65}, Y. Hu¹, Z. M. Hu⁶⁰, G. S. Huang^{73,59}, K. X. Huang⁶⁰, L. Q. Huang^{32,65}, P. Huang⁴³, X. T. Huang⁵¹, Y. P. Huang¹, Y. S. Huang⁶⁰, T. Hussain⁷⁵, N. Hüsken³⁶, N. in der Wiesche⁷⁰, J. Jackson²⁸, Q. Ji¹, Q. P. Ji²⁰, W. Ji^{1,65}, X. B. Ji^{1,65}, X. L. Ji^{1,59}, Y. Y. Ji⁵¹, Z. K. Jia^{73,59}, D. Jiang^{1,65}, H. B. Jiang⁷⁸, P. C. Jiang^{47,h}, S. J. Jiang⁹, T. J. Jiang¹⁷, X. S. Jiang^{1,59,65}, Y. Jiang⁶⁵, J. B. Jiao⁵¹, J. K. Jiao³⁵, Z. Jiao²⁴, S. Jin⁴³, Y. Jin⁶⁸, M. Q. Jing^{1,65}, X. M. Jing⁶⁵, T. Johansson⁷⁷, S. Kabana³⁴, N. Kalantar-Nayestanaki⁶⁶, X. L. Kang⁹, X. S. Kang⁴¹, M. Kavatsyuk⁶⁶, B. C. Ke⁸², V. Khachatryan²⁸, A. Khoukaz⁷⁰, R. Kiuchi¹, O. B. Kolcu^{63A}, B. Kopf³, M. Kuessner³, X. Kui^{1,65}, N. Kumar²⁷, A. Kupsc^{45,77}, W. Kühn³⁸, Q. Lan⁷⁴, W. N. Lan²⁰, T. T. Lei^{73,59}, M. Lellmann³⁶, T. Lenz³⁶, C. Li^{73,59}, C. Li⁴⁴, C. Li⁴⁸, C. H. Li⁴⁰, C. K. Li²¹, D. M. Li⁸², F. Li^{1,59}, G. Li¹, H. B. Li^{1,65}, H. J. Li²⁰, H. N. Li^{57,j}, Hui Li⁴⁴, J. R. Li⁶², J. S. Li⁶⁰, K. Li¹, K. L. Li²⁰, K. L. Li^{39,k,l}, L. J. Li^{1,65}, Lei Li⁴⁹, M. H. Li⁴⁴, M. R. Li^{1,65}, P. L. Li⁶⁵, P. R. Li^{39,k,l}, Q. M. Li^{1,65}, Q. X. Li⁵¹, R. Li^{18,32}, S. X. Li¹², T. Li⁵¹, T. Y. Li⁴⁴, W. D. Li^{1,65}, W. G. Li^{1,a}, X. Li^{1,65}, X. H. Li^{73,59}, X. L. Li⁵¹, X. Y. Li^{1,8}, X. Z. Li⁶⁰, Y. Li²⁰, Y. G. Li^{47,h}, Y. P. Li³⁵, Z. J. Li⁶⁰, Z. Y. Li⁸⁰, H. Liang^{73,59}, Y. F. Liang⁵⁵, Y. T. Liang^{32,65}, G. R. Liao¹⁴, L. B. Liao⁶⁰, M. H. Liao⁶⁰, Y. P. Liao^{1,65}, J. Libby²⁷, A. Limphirat⁶¹, C. C. Lin⁵⁶, D. X. Lin^{32,65}, L. Q. Lin⁴⁰, T. Lin¹, B. J. Liu¹, B. X. Liu⁷⁸, C. Liu³⁵, C. X. Liu¹, F. Liu¹, F. H. Liu⁵⁴, Feng Liu⁶, G. M. Liu^{57,j}, H. Liu^{39,k,l}, H. B. Liu¹⁵, H. H. Liu¹, H. M. Liu^{1,65}, Huihui Liu²², J. B. Liu^{73,59}, J. J. Liu²¹, K. Liu⁷⁴, K. Liu^{39,k,l}, K. Y. Liu⁴¹, Ke Liu²³, L. C. Liu⁴⁴, Lu Liu⁴⁴, M. H. Liu^{12,g}, P. L. Liu¹, Q. Liu⁶⁵, S. B. Liu^{73,59}, T. Liu^{12,g}, W. K. Liu⁴⁴, W. M. Liu^{73,59}, W. T. Liu⁴⁰, X. Liu⁴⁰, X. Liu^{39,k,l}, X. K. Liu^{39,k,l}, X. Y. Liu⁷⁸, Y. Liu⁸², Y. Liu⁸², Y. Liu^{39,k,l}, Y. B. Liu⁴⁴, Z. A. Liu^{1,59,65}, Z. D. Liu⁹, Z. Q. Liu⁵¹, X. C. Lou^{1,59,65}, F. X. Lu⁶⁰, H. J. Lu²⁴, J. G. Lu^{1,59}, X. L. Lu¹⁶, Y. Lu⁷, Y. H. Lu^{1,65}, Y. P. Lu^{1,59}, Z. H. Lu^{1,65}, C. L. Luo⁴², J. R. Luo⁶⁰, J. S. Luo^{1,65}, M. X. Luo⁸¹, T. Luo^{12,g}, X. L. Luo^{1,59}, Z. Y. Lv²³, X. R. Lyu^{65,p}, Y. F. Lyu⁴⁴, Y. H. Lyu⁸², F. C. Ma⁴¹, H. L. Ma¹, J. L. Ma^{1,65}, L. L. Ma⁵¹, L. R. Ma⁶⁸, Q. M. Ma¹, R. Q. Ma^{1,65}, R. Y. Ma²⁰, T. Ma^{73,59}, X. T. Ma^{1,65}, X. Y. Ma^{1,59}, Y. M. Ma³², F. E. Maas¹⁹, I. MacKay⁷¹, M. Maggiora^{76A,76C}, S. Malde⁷¹, Q. A. Malik⁷⁵, H. X. Mao^{39,k,l}, Y. J. Mao^{47,h}, Z. P. Mao¹, S. Marcello^{76A,76C}, A. Marshall⁶⁴, F. M. Melendi^{30A,30B}, Y. H. Meng⁶⁵, Z. X. Meng⁶⁸, G. Mezzadri^{30A}, H. Miao^{1,65}, T. J. Min⁴³, R. E. Mitchell²⁸, X. H. Mo^{1,59,65}, B. Moses²⁸, N. Yu. Muchnoi^{4,c}, J. Muskalla³⁶, Y. Nefedov³⁷, F. Nerling^{19,e}, L. S. Nie²¹, I. B. Nikolaev^{4,c}, Z. Ning^{1,59}, S. Nisar^{11,m}, Q. L. Niu^{39,k,l}, W. D. Niu^{12,g}, C. Normand⁶⁴, S. L. Olsen^{10,65}, Q. Ouyang^{1,59,65}, S. Pacetti^{29B,29C}, X. Pan⁵⁶, Y. Pan⁵⁸, A. Pathak¹⁰, Y. P. Pei^{73,59}, M. Pelizaeus³, H. P. Peng^{73,59}, X. J. Peng^{39,k,l}, Y. Y. Peng^{39,k,l}, K. Peters^{13,e}, K. Petridis⁶⁴, J. L. Ping⁴², R. G. Ping^{1,65}, S. Plura³⁶, V. Prasad³⁵, F. Z. Qi¹, H. R. Qi⁶², M. Qi⁴³, S. Qian^{1,59}, W. B. Qian⁶⁵, C. F. Qiao⁶⁵, J. H. Qiao²⁰, J. J. Qin⁷⁴, J. L. Qin⁵⁶, L. Q. Qin¹⁴, L. Y. Qin^{73,59}, P. B. Qin⁷⁴, X. P. Qin^{12,g}, X. S. Qin⁵¹, Z. H. Qin^{1,59}, J. F. Qiu¹, Z. H. Qu⁷⁴, J. Rademacker⁶⁴, C. F. Redmer³⁶, A. Rivetti^{76C}, M. Roloff^{76C}, G. Rong^{1,65}, S. S. Rong^{1,65}, F. Rosini^{29B,29C}, Ch. Rosner¹⁹, M. Q. Ruan^{1,59}, N. Salone⁴⁵, A. Sarantsev^{37,d}, Y. Schelhaas³⁶, K. Schoenning⁷⁷, M. Scodellaggio^{30A}, K. Y. Shan^{12,g}, W. Shan²⁵, X. Y. Shan^{73,59}, Z. J. Shang^{39,k,l}, J. F. Shangguan¹⁷, L. G. Shao^{1,65}, M. Shao^{73,59}, C. P. Shen^{12,g}, H. F. Shen^{1,8}, W. H. Shen⁶⁵, X. Y. Shen^{1,65}, B. A. Shi⁶⁵, H. Shi^{73,59}, J. L. Shi^{12,g}, J. Y. Shi¹, S. Y. Shi⁷⁴, X. Shi^{1,59}, H. L. Song^{73,59}, J. J. Song²⁰, T. Z. Song⁶⁰, W. M. Song³⁵, Y. J. Song^{12,g}, Y. X. Song^{47,h,n}, S. Sosio^{76A,76C}, S. Spataro^{76A,76C}, F. Stieler³⁶, S. S. Su⁴¹, Y. J. Su⁶⁵, G. B. Sun⁷⁸, G. X. Sun¹, H. Sun⁶⁵, H. K. Sun¹, J. F. Sun²⁰, K. Sun⁶², L. Sun⁷⁸, S. S. Sun^{1,65}, T. Sun^{52,f}, Y. C. Sun⁷⁸, Y. H. Sun³¹, Y. J. Sun^{73,59}, Y. Z. Sun¹, Z. Q. Sun^{1,65}, Z. T. Sun⁵¹, C. J. Tang⁵⁵, G. Y. Tang¹, J. Tang⁶⁰, J. J. Tang^{73,59}, L. F. Tang⁴⁰, Y. A. Tang⁷⁸, L. Y. Tao⁷⁴, M. Tat⁷¹, J. X. Teng^{73,59}, J. Y. Tian^{73,59}, W. H. Tian⁶⁰, Y. Tian³², Z. F. Tian⁷⁸, I. Uman^{63B}, B. Wang⁶⁰, B. Wang¹, Bo Wang^{73,59}, C. Wang^{39,k,l}, C. Wang²⁰, Cong Wang²³, D. Y. Wang^{47,h}, H. J. Wang^{39,k,l}, J. J. Wang⁷⁸, K. Wang^{1,59}, L. L. Wang¹, L. W. Wang³⁵, M. Wang⁵¹, M. Wang^{73,59}, N. Y. Wang⁶⁵, S. Wang^{12,g}, T. Wang^{12,g}, T. J. Wang⁴⁴, W. Wang⁶⁰, W. Wang⁷⁴, W. P. Wang^{36,59,73,o}, X. Wang^{47,h}, X. F. Wang^{39,k,l}, X. J. Wang⁴⁰, X. L. Wang^{12,g}, X. N. Wang¹, Y. Wang⁶², Y. D. Wang⁴⁶, Y. F. Wang^{1,8,65}, Y. H. Wang^{39,k,l}, Y. J. Wang^{73,59}, Y. L. Wang²⁰, Y. N. Wang⁷⁸, Y. Q. Wang¹, Yaqian Wang¹⁸, Yi Wang⁶², Yuan Wang^{18,32}, Z. Wang^{1,59}, Z. L. Wang², Z. L. Wang⁷⁴, Z. Q. Wang^{12,g}, Z. Y. Wang^{1,65}, D. H. Wei¹⁴, H. R. Wei⁴⁴, F. Weidner⁷⁰, S. P. Wen¹, Y. R. Wen⁴⁰, U. Wiedner³, G. Wilkinson⁷¹, M. Wolke⁷⁷, C. Wu⁴⁰, J. F. Wu^{1,8}, L. H. Wu¹, L. J. Wu²⁰, L. J. Wu^{1,65},

Lianjie Wu²⁰, S. G. Wu^{1,65}, S. M. Wu⁶⁵, X. Wu^{12,g}, X. H. Wu³⁵, Y. J. Wu³², Z. Wu^{1,59}, L. Xia^{73,59}, X. M. Xian⁴⁰, B. H. Xiang^{1,65}, D. Xiao^{39,k,l}, G. Y. Xiao⁴³, H. Xiao⁷⁴, Y. L. Xiao^{12,g}, Z. J. Xiao⁴², C. Xie⁴³, K. J. Xie^{1,65}, X. H. Xie^{47,h}, Y. Xie⁵¹, Y. G. Xie^{1,59}, Y. H. Xie⁶, Z. P. Xie^{73,59}, T. Y. Xing^{1,65}, C. F. Xu^{1,65}, C. J. Xu⁶⁰, G. F. Xu¹, H. Y. Xu^{68,2}, H. Y. Xu², M. Xu^{73,59}, Q. J. Xu¹⁷, Q. N. Xu³¹, T. D. Xu⁷⁴, W. Xu¹, W. L. Xu⁶⁸, X. P. Xu⁵⁶, Y. Xu⁴¹, Y. Xu^{12,g}, Y. C. Xu⁷⁹, Z. S. Xu⁶⁵, F. Yan^{12,g}, H. Y. Yan⁴⁰, L. Yan^{12,g}, W. B. Yan^{73,59}, W. C. Yan⁸², W. H. Yan⁶, W. P. Yan²⁰, X. Q. Yan^{1,65}, H. J. Yang^{52,f}, H. L. Yang³⁵, H. X. Yang¹, J. H. Yang⁴³, R. J. Yang²⁰, T. Yang¹, Y. Yang^{12,g}, Y. F. Yang⁴⁴, Y. H. Yang⁴³, Y. Q. Yang⁹, Y. X. Yang^{1,65}, Y. Z. Yang²⁰, M. Ye^{1,59}, M. H. Ye^{8,a}, Z. J. Ye^{57,j}, Junhao Yin⁴⁴, Z. Y. You⁶⁰, B. X. Yu^{1,59,65}, C. X. Yu⁴⁴, G. Yu¹³, J. S. Yu^{26,i}, L. Q. Yu^{12,g}, M. C. Yu⁴¹, T. Yu⁷⁴, X. D. Yu^{47,h}, Y. C. Yu⁸², C. Z. Yuan^{1,65}, H. Yuan^{1,65}, J. Yuan³⁵, J. Yuan⁴⁶, L. Yuan², S. C. Yuan^{1,65}, X. Q. Yuan¹, Y. Yuan^{1,65}, Z. Y. Yuan⁶⁰, C. X. Yue⁴⁰, Ying Yue²⁰, A. A. Zafar⁷⁵, S. H. Zeng^{64A,64B,64C,64D}, X. Zeng^{12,g}, Y. Zeng^{26,i}, Y. J. Zeng^{1,65}, Y. J. Zeng⁶⁰, X. Y. Zhai³⁵, Y. H. Zhan⁶⁰, A. Q. Zhang^{1,65}, B. L. Zhang^{1,65}, B. X. Zhang¹, D. H. Zhang⁴⁴, G. Y. Zhang²⁰, G. Y. Zhang^{1,65}, H. Zhang^{73,59}, H. Zhang⁸², H. C. Zhang^{1,59,65}, H. H. Zhang⁶⁰, H. Q. Zhang^{1,59,65}, H. R. Zhang^{73,59}, H. Y. Zhang^{1,59}, J. Zhang⁶⁰, J. Zhang⁸², J. J. Zhang⁵³, J. L. Zhang²¹, J. Q. Zhang⁴², J. S. Zhang^{12,g}, J. W. Zhang^{1,59,65}, J. X. Zhang^{39,k,l}, J. Y. Zhang¹, J. Z. Zhang^{1,65}, Jianyu Zhang⁶⁵, L. M. Zhang⁶², Lei Zhang⁴³, N. Zhang⁸², P. Zhang^{1,8}, Q. Zhang²⁰, Q. Y. Zhang³⁵, R. Y. Zhang^{39,k,l}, S. H. Zhang^{1,65}, Shulei Zhang^{26,i}, X. M. Zhang¹, X. Y. Zhang⁴¹, X. Y. Zhang⁵¹, Y. Zhang⁷⁴, Y. Zhang¹, Y. T. Zhang⁸², Y. H. Zhang^{1,59}, Y. M. Zhang⁴⁰, Y. P. Zhang^{73,59}, Z. D. Zhang¹, Z. H. Zhang¹, Z. L. Zhang⁵⁶, Z. L. Zhang³⁵, Z. X. Zhang²⁰, Z. Y. Zhang⁴⁴, Z. Y. Zhang⁷⁸, Z. Z. Zhang⁴⁶, Zh. Zh. Zhang²⁰, G. Zhao¹, J. Y. Zhao^{1,65}, J. Z. Zhao^{1,59}, L. Zhao^{73,59}, L. Zhao¹, M. G. Zhao⁴⁴, N. Zhao⁸⁰, R. P. Zhao⁶⁵, S. J. Zhao⁸², Y. B. Zhao^{1,59}, Y. L. Zhao⁵⁶, Y. X. Zhao^{32,65}, Z. G. Zhao^{73,59}, A. Zhemchugov^{37,b}, B. Zheng⁷⁴, B. M. Zheng³⁵, J. P. Zheng^{1,59}, W. J. Zheng^{1,65}, X. R. Zheng²⁰, Y. H. Zheng^{65,p}, B. Zhong⁴², C. Zhong²⁰, H. Zhou^{36,51,o}, J. Q. Zhou³⁵, J. Y. Zhou³⁵, S. Zhou⁶, X. Zhou⁷⁸, X. K. Zhou⁶, X. R. Zhou^{73,59}, X. Y. Zhou⁴⁰, Y. X. Zhou⁷⁹, Y. Z. Zhou^{12,g}, A. N. Zhu⁶⁵, J. Zhu⁴⁴, K. Zhu¹, K. J. Zhu^{1,59,65}, K. S. Zhu^{12,g}, L. Zhu³⁵, L. X. Zhu⁶⁵, S. H. Zhu⁷², T. J. Zhu^{12,g}, W. D. Zhu^{12,g}, W. D. Zhu⁴², W. J. Zhu¹, W. Z. Zhu²⁰, Y. C. Zhu^{73,59}, Z. A. Zhu^{1,65}, X. Y. Zhuang⁴⁴, J. H. Zou¹, J. Zu^{73,59}

(BESIII Collaboration)

¹ Institute of High Energy Physics, Beijing 100049, People's Republic of China

² Beihang University, Beijing 100191, People's Republic of China

³ Bochum Ruhr-University, D-44780 Bochum, Germany

⁴ Budker Institute of Nuclear Physics SB RAS (BINP), Novosibirsk 630090, Russia

⁵ Carnegie Mellon University, Pittsburgh, Pennsylvania 15213, USA

⁶ Central China Normal University, Wuhan 430079, People's Republic of China

⁷ Central South University, Changsha 410083, People's Republic of China

⁸ China Center of Advanced Science and Technology, Beijing 100190, People's Republic of China

⁹ China University of Geosciences, Wuhan 430074, People's Republic of China

¹⁰ Chung-Ang University, Seoul, 06974, Republic of Korea

¹¹ COMSATS University Islamabad, Lahore Campus, Defence Road, Off Raiwind Road, 54000 Lahore, Pakistan

¹² Fudan University, Shanghai 200433, People's Republic of China

¹³ GSI Helmholtzcentre for Heavy Ion Research GmbH, D-64291 Darmstadt, Germany

¹⁴ Guangxi Normal University, Guilin 541004, People's Republic of China

¹⁵ Guangxi University, Nanning 530004, People's Republic of China

¹⁶ Guangxi University of Science and Technology, Liuzhou 545006, People's Republic of China

¹⁷ Hangzhou Normal University, Hangzhou 310036, People's Republic of China

¹⁸ Hebei University, Baoding 071002, People's Republic of China

¹⁹ Helmholtz Institute Mainz, Staudinger Weg 18, D-55099 Mainz, Germany

²⁰ Henan Normal University, Xinxiang 453007, People's Republic of China

²¹ Henan University, Kaifeng 475004, People's Republic of China

²² Henan University of Science and Technology, Luoyang 471003, People's Republic of China

²³ Henan University of Technology, Zhengzhou 450001, People's Republic of China

²⁴ Huangshan College, Huangshan 245000, People's Republic of China

²⁵ Hunan Normal University, Changsha 410081, People's Republic of China

²⁶ Hunan University, Changsha 410082, People's Republic of China

²⁷ Indian Institute of Technology Madras, Chennai 600036, India

²⁸ Indiana University, Bloomington, Indiana 47405, USA

²⁹ INFN Laboratori Nazionali di Frascati, (A)INFN Laboratori Nazionali di Frascati, I-00044, Frascati, Italy; (B)INFN Sezione di Perugia, I-06100, Perugia, Italy; (C)University of Perugia, I-06100, Perugia, Italy

³⁰ INFN Sezione di Ferrara, (A)INFN Sezione di Ferrara, I-44122, Ferrara, Italy; (B)University of Ferrara, I-44122, Ferrara, Italy

³¹ Inner Mongolia University, Hohhot 010021, People's Republic of China

³² Institute of Modern Physics, Lanzhou 730000, People's Republic of China

³³ Institute of Physics and Technology, Mongolian Academy of Sciences, Peace Avenue 54B, Ulaanbaatar 13330, Mongolia

³⁴ Instituto de Alta Investigación, Universidad de Tarapacá, Casilla 7D, Arica 1000000, Chile

³⁵ Jilin University, Changchun 130012, People's Republic of China

³⁶ Johannes Gutenberg University of Mainz, Johann-Joachim-Becher-Weg 45, D-55099 Mainz, Germany

³⁷ Joint Institute for Nuclear Research, 141980 Dubna, Moscow region, Russia
³⁸ Justus-Liebig-Universitaet Giessen, II. Physikalisches Institut, Heinrich-Buff-Ring 16, D-35392 Giessen, Germany
³⁹ Lanzhou University, Lanzhou 730000, People's Republic of China
⁴⁰ Liaoning Normal University, Dalian 116029, People's Republic of China
⁴¹ Liaoning University, Shenyang 110036, People's Republic of China
⁴² Nanjing Normal University, Nanjing 210023, People's Republic of China
⁴³ Nanjing University, Nanjing 210093, People's Republic of China
⁴⁴ Nankai University, Tianjin 300071, People's Republic of China
⁴⁵ National Centre for Nuclear Research, Warsaw 02-093, Poland
⁴⁶ North China Electric Power University, Beijing 102206, People's Republic of China
⁴⁷ Peking University, Beijing 100871, People's Republic of China
⁴⁸ Qufu Normal University, Qufu 273165, People's Republic of China
⁴⁹ Renmin University of China, Beijing 100872, People's Republic of China
⁵⁰ Shandong Normal University, Jinan 250014, People's Republic of China
⁵¹ Shandong University, Jinan 250100, People's Republic of China
⁵² Shanghai Jiao Tong University, Shanghai 200240, People's Republic of China
⁵³ Shanxi Normal University, Linfen 041004, People's Republic of China
⁵⁴ Shanxi University, Taiyuan 030006, People's Republic of China
⁵⁵ Sichuan University, Chengdu 610064, People's Republic of China
⁵⁶ Soochow University, Suzhou 215006, People's Republic of China
⁵⁷ South China Normal University, Guangzhou 510006, People's Republic of China
⁵⁸ Southeast University, Nanjing 211100, People's Republic of China
⁵⁹ State Key Laboratory of Particle Detection and Electronics, Beijing 100049, Hefei 230026, People's Republic of China
⁶⁰ Sun Yat-Sen University, Guangzhou 510275, People's Republic of China
⁶¹ Suranaree University of Technology, University Avenue 111, Nakhon Ratchasima 30000, Thailand
⁶² Tsinghua University, Beijing 100084, People's Republic of China
⁶³ Turkish Accelerator Center Particle Factory Group, (A)Istanbul University, 34010, Istanbul, Turkey; (B)Near East University, Nicosia, North Cyprus, 99138, Mersin 10, Turkey
⁶⁴ University of Bristol, H H Wills Physics Laboratory, Tyndall Avenue, Bristol, BS8 1TL, UK
⁶⁵ University of Chinese Academy of Sciences, Beijing 100049, People's Republic of China
⁶⁶ University of Groningen, NL-9747 AA Groningen, The Netherlands
⁶⁷ University of Hawaii, Honolulu, Hawaii 96822, USA
⁶⁸ University of Jinan, Jinan 250022, People's Republic of China
⁶⁹ University of Manchester, Oxford Road, Manchester, M13 9PL, United Kingdom
⁷⁰ University of Muenster, Wilhelm-Klemm-Strasse 9, 48149 Muenster, Germany
⁷¹ University of Oxford, Keble Road, Oxford OX13RH, United Kingdom
⁷² University of Science and Technology Liaoning, Anshan 114051, People's Republic of China
⁷³ University of Science and Technology of China, Hefei 230026, People's Republic of China
⁷⁴ University of South China, Hengyang 421001, People's Republic of China
⁷⁵ University of the Punjab, Lahore-54590, Pakistan
⁷⁶ University of Turin and INFN, (A)University of Turin, I-10125, Turin, Italy; (B)University of Eastern Piedmont, I-15121, Alessandria, Italy; (C)INFN, I-10125, Turin, Italy
⁷⁷ Uppsala University, Box 516, SE-75120 Uppsala, Sweden
⁷⁸ Wuhan University, Wuhan 430072, People's Republic of China
⁷⁹ Yantai University, Yantai 264005, People's Republic of China
⁸⁰ Yunnan University, Kunming 650500, People's Republic of China
⁸¹ Zhejiang University, Hangzhou 310027, People's Republic of China
⁸² Zhengzhou University, Zhengzhou 450001, People's Republic of China

^a Deceased
^b Also at the Moscow Institute of Physics and Technology, Moscow 141700, Russia
^c Also at the Novosibirsk State University, Novosibirsk, 630090, Russia
^d Also at the NRC "Kurchatov Institute", PNPI, 188300, Gatchina, Russia
^e Also at Goethe University Frankfurt, 60323 Frankfurt am Main, Germany
^f Also at Key Laboratory for Particle Physics, Astrophysics and Cosmology, Ministry of Education; Shanghai Key Laboratory for Particle Physics and Cosmology; Institute of Nuclear and Particle Physics, Shanghai 200240, People's Republic of China
^g Also at Key Laboratory of Nuclear Physics and Ion-beam Application (MOE) and Institute of Modern Physics, Fudan University, Shanghai 200443, People's Republic of China
^h Also at State Key Laboratory of Nuclear Physics and Technology, Peking University, Beijing 100871, People's Republic of China
ⁱ Also at School of Physics and Electronics, Hunan University, Changsha 410082, China
^j Also at Guangdong Provincial Key Laboratory of Nuclear Science, Institute of Quantum Matter, South China Normal University, Guangzhou 510006, China
^k Also at MOE Frontiers Science Center for Rare Isotopes, Lanzhou University, Lanzhou 730000, People's Republic of China

^l Also at Lanzhou Center for Theoretical Physics, Lanzhou University, Lanzhou 730000, People's Republic of China

^m Also at the Department of Mathematical Sciences, IBA, Karachi 75270, Pakistan

ⁿ Also at Ecole Polytechnique Federale de Lausanne (EPFL), CH-1015 Lausanne, Switzerland

^o Also at Helmholtz Institute Mainz, Staudinger Weg 18, D-55099 Mainz, Germany

^p Also at Hangzhou Institute for Advanced Study, University of Chinese Academy of Sciences, Hangzhou 310024, China

Based on a sample of $2.7 \times 10^9 \psi(3686)$ events collected by the BESIII detector operating at the BEPCII collider, an analysis of the decay $\psi(3686) \rightarrow \gamma\chi_{cJ}, \chi_{cJ} \rightarrow \eta\eta\eta'$ is performed. The decay modes χ_{c1} and $\chi_{c2} \rightarrow \eta\eta\eta'$ are observed for the first time, and their corresponding branching fractions are determined to be $\mathcal{B}(\chi_{c1} \rightarrow \eta\eta\eta') = (1.39 \pm 0.13(\text{stat.}) \pm 0.09(\text{sys.})) \times 10^{-4}$ and $\mathcal{B}(\chi_{c2} \rightarrow \eta\eta\eta') = (4.42 \pm 0.86(\text{stat.}) \pm 0.37(\text{sys.})) \times 10^{-5}$. An upper limit on the branching fraction of $\chi_{c0} \rightarrow \eta\eta\eta'$ is set as 2.64×10^{-5} at 90% confidence level (CL). A partial wave analysis (PWA) of the decay $\chi_{c1} \rightarrow \eta\eta\eta'$ is performed to search for the 1^{-+} exotic state $\eta_1(1855)$. The PWA result indicates that the structure in the $\eta\eta'$ mass spectrum is mainly attributed to the $f_0(1500)$, while in the $\eta\eta$ mass spectrum, it is primarily the 0^{++} phase space. The upper limit of $\mathcal{B}(\chi_{c1} \rightarrow \eta_1(1855)\eta) \cdot \mathcal{B}(\eta_1(1855) \rightarrow \eta\eta') < 9.79 \times 10^{-5}$ is set based on the PWA at 90% CL.

I. INTRODUCTION

The quark model describes mesons as composed of a quark and an antiquark ($q\bar{q}$), while quantum chromodynamics (QCD) allows the existence of exotic states. Exploring spin-exotic states is an important area of research. These states have exotic quantum numbers beyond those in the quark model, such as $J^{PC} = 0^{--}$, 0^{+-} , and 0^{-+} , which can be easily identified.

A hybrid is an exotic state composed of a quark, an antiquark and an excited gluon field, which reflects the gluonic degrees of freedom. The 1^{-+} hybrid state, predicted by lattice QCD (LQCD) as the lightest hadron with spin-exotic quantum numbers, is estimated to have a mass in 1.7-2.1 GeV/ c^2 [1]. LQCD has recently investigated the production of 1^{-+} hybrid in J/ψ radiative decay and its possible decay modes [2, 3]. The isovector state $\pi_1(1600)$ has long been considered an experimental candidate for the 1^{-+} spin-exotic nonet [4-7]. CLEO-c has found a clear P-wave signal in the $\eta'\pi^\pm$ system around 1.6 GeV/ c^2 from the $\chi_{c1} \rightarrow \eta'\pi^+\pi^-$ process [8]. Recently, the 1^{-+} isoscalar state $\eta_1(1855)$ was discovered in the $\eta\eta'$ system by BESIII via $J/\psi \rightarrow \gamma\eta\eta'$ [9, 10] and it is considered to be a partner of $\pi_1(1600)$, marking a new research direction for spin-exotic states. These research results help in understanding the production mechanism of the 1^{-+} spin-exotic state. It is possible to observe $\eta_1(1855)$ via $\chi_{c1} \rightarrow \eta_1(1855)\eta$, with $\eta_1(1855) \rightarrow \eta\eta'$.

In this paper, based on a sample of $2.7 \times 10^9 \psi(3686)$ events collected by the BESIII detector [11], an analysis of the decay $\psi(3686) \rightarrow \gamma\chi_{cJ}, \chi_{cJ} \rightarrow \eta\eta\eta'$ is performed to search for $\eta_1(1855)$. The η' is reconstructed via $\eta' \rightarrow \gamma\pi^+\pi^-$ and $\eta' \rightarrow \eta\pi^+\pi^-$, and the η is reconstructed via $\gamma\gamma$.

II. BESIII DETECTOR AND MONTE CARLO SIMULATION

The BESIII detector [11] records symmetric e^+e^- collisions provided by the BEPCII storage ring [12], with a center-of-mass energy ranging from 1.84 to 4.95 GeV

and a peak luminosity of $1.1 \times 10^{33} \text{ cm}^{-2}\text{s}^{-1}$ achieved at $\sqrt{s} = 3.773$ GeV. BESIII has collected large data samples in this energy region [13]. The cylindrical core of the BESIII detector covers 93% of the full solid angle and consists of a helium-based multilayer drift chamber (MDC), a time-of-flight system (TOF), and a CsI(Tl) electromagnetic calorimeter (EMC), which are all enclosed in a superconducting solenoidal magnet providing a 1.0 T magnetic field. The solenoid is supported by an octagonal flux-return yoke with resistive plate counter muon identification modules interleaved with steel. The charged-particle momentum resolution at 1 GeV/ c is 0.5%, and the resolution of the specific ionization energy (dE/dx) is 6% for electrons from Bhabha scattering. The EMC measures photon energies with a resolution of 2.5% (5%) at 1 GeV in the barrel (end-cap) region. The time resolution in the TOF plastic scintillator barrel region is 68 ps, while that in the end-cap region was 110 ps. The end-cap TOF system was upgraded in 2015 using multi-gap resistive plate chamber technology, providing a time resolution of 60 ps, which benefits 85% of the data used in this analysis [14-16].

Monte Carlo (MC) simulated samples, produced with GEANT4-based [17] software, which includes the geometric description of the BESIII detector and the detector response, are used to determine detection efficiencies and to estimate backgrounds. The simulation models the beam energy spread and initial state radiation (ISR) in the e^+e^- annihilations with the generator KKMC [18, 19]. The inclusive MC sample includes the production of the $\psi(3686)$ resonance, the ISR production of the J/ψ , and the continuum processes incorporated in KKMC [18, 19]. Known decay modes are modeled with EVTGEN [20, 21] using branching fractions taken from the Particle Data Group (PDG) [22]. The remaining unknown charmonium decays are modeled with LUNDCHARM [23, 24]. Final state radiation (FSR) from charged final state particles is incorporated using PHOTOS package [25]. Exclusive MC samples are generated to determine the detection efficiency and optimize selection criteria. The signal is simulated with the E1 transition $\psi(3686) \rightarrow \gamma\chi_{cJ}$, where the polar angle ϕ of the radiative photon in the e^+e^- center-of-

mass frame is distributed according to $(1 + \lambda \cos^2 \theta)$. For $J = 0, 1$ and 2 , λ is set to be $1, -\frac{1}{3}$ and $\frac{1}{13}$, respectively [20, 21]. The decay $\eta' \rightarrow \gamma\pi^+\pi^-$ is simulated by a model that considers both the $\rho - \omega$ interference and the box anomaly [26], while the decay $\eta' \rightarrow \eta\pi^+\pi^-$ is simulated with a model based on the measured matrix elements [27]. Other processes are generated uniformly in phase space (PHSP).

III. EVENT SELECTION

Charged tracks detected in the MDC are required to have a polar angle (θ) within the range of $|\cos \theta| < 0.93$, where θ is defined with respect to the z -axis, the symmetry axis of the MDC. The distance of the closest approach to the interaction point (IP) must be less than 10 cm along the z -axis, and less than 1 cm in the transverse plane. Two good charged tracks are required in the final state, and the total charge must be equal to zero.

The particle identification (PID) for charged tracks combines measurements of the dE/dx in the MDC and the flight time in the TOF to form likelihoods $\mathcal{L}(h)$ ($h = p, K, \pi$) for each hadron (h) hypothesis. A charged track is identified as a pion when the pion hypothesis yields the maximum likelihood value, i.e. $\mathcal{L}(\pi) > \mathcal{L}(K)$, and $\mathcal{L}(\pi) > \mathcal{L}(p)$. The two good charged tracks must both be identified as pions.

In the selection of good photon candidates, the deposited energy for a cluster is required to be larger than 25 MeV in the barrel ($|\cos \theta| < 0.80$) or 50 MeV in the end-cap ($0.86 < |\cos \theta| < 0.92$) regions. To exclude spurious photons caused by hadronic interactions and final state radiation, photon candidates must be at least 10° away from any charged tracks when extrapolated to the EMC. To suppress electronic noise and unrelated showers, the difference between the EMC time and the event start time is required to be within $[0, 700]$ ns.

For the $\psi(3686) \rightarrow \gamma\chi_{cJ}$, $\chi_{cJ} \rightarrow \eta\eta\eta'$, $\eta' \rightarrow \gamma\pi^+\pi^-$ mode, events are reconstructed with two oppositely charged tracks and at least six candidate photons. A six-constraint (6C) kinematic fit under the hypothesis of $\psi(3686) \rightarrow \gamma\gamma\eta\eta\pi^+\pi^-$ is performed by imposing the energy-momentum conservation and constraining the mass of each pair of photons to the nominal η mass from the PDG [22]. If there is more than one combination, the one with the minimum χ^2 value of the fit (denoted as χ^2_{6C}) is retained. The result χ^2_{6C} is required to be less than 20, which is obtained by optimizing the figure of merit (FOM). The FOM is defined as $\text{FOM} = \frac{S}{\sqrt{S+B}}$, where S is the normalized number of signal events in the signal MC samples and $(S+B)$ corresponds to the number of data events. To suppress backgrounds with five or seven photons in the final state, 4C kinematic fits are performed by imposing the energy-momentum conservation under the hypotheses of $\psi(3686) \rightarrow 5\gamma\pi^+\pi^-$, $\psi(3686) \rightarrow 6\gamma\pi^+\pi^-$ and $\psi(3686) \rightarrow 7\gamma\pi^+\pi^-$. The $\chi^2_{4C}(6\gamma\pi^+\pi^-)$ is required to be less than all possible

$\chi^2_{4C}(5\gamma\pi^+\pi^-)$ and $\chi^2_{4C}(7\gamma\pi^+\pi^-)$. To reconstruct the η' candidate, the $\gamma\pi^+\pi^-$ combination with the minimum $|M(\gamma\pi^+\pi^-) - m_{\eta'}|$ is selected, where $m_{\eta'}$ is the nominal η' mass taken from the PDG [22]. Events with $|M(\gamma\pi^+\pi^-) - m_{\eta'}| < 0.01 \text{ GeV}/c^2$ are selected for further analysis. To suppress backgrounds containing π^0 , events with $|M(\gamma\gamma) - m_{\pi^0}| < 0.02 \text{ GeV}/c^2$ are rejected, where $M(\gamma\gamma)$ is the invariant mass of each photon pair except the two-photon pairs assigned to the η , and m_{π^0} is the nominal π^0 mass [22]. The invariant mass distribution of $\gamma\pi^+\pi^-$ is shown in Fig. 1(a).

For the decays $\psi(3686) \rightarrow \gamma\chi_{cJ}$, $\chi_{cJ} \rightarrow \eta\eta\eta'$, $\eta' \rightarrow \eta\pi^+\pi^-$, events are reconstructed with two oppositely charged tracks and at least seven candidate photons. A seven-constraint (7C) kinematic fit under the hypothesis of $\psi(3686) \rightarrow \gamma\eta\eta\eta\pi^+\pi^-$ is performed by imposing the energy-momentum conservation and constraining the mass of each pair of photons to m_η . If there is more than one combination, the one with the minimum χ^2 value of the fit (denoted as χ^2_{7C}) is retained. The result χ^2_{7C} is required to be less than 55, which is obtained by optimizing the FOM, similarly to the optimization performed for the $\eta' \rightarrow \gamma\pi^+\pi^-$ mode. To suppress backgrounds with eight photons in the final state, 4C kinematic fits are performed by imposing the energy-momentum conservation under the hypotheses of $\psi(3686) \rightarrow 6\gamma\pi^+\pi^-$, $\psi(3686) \rightarrow 7\gamma\pi^+\pi^-$ and $\psi(3686) \rightarrow 8\gamma\pi^+\pi^-$. Since $\chi^2_{4C}(6\gamma\pi^+\pi^-)$ has no effect on the number of data events, $\chi^2_{4C}(7\gamma\pi^+\pi^-)$ is required to be less than $\chi^2_{4C}(8\gamma\pi^+\pi^-)$. The $\eta\pi^+\pi^-$ combination with the minimum $|M(\eta\pi^+\pi^-) - m_{\eta'}|$ is used to reconstruct the η' candidate. Events with $|M(\eta\pi^+\pi^-) - m_{\eta'}| < 0.01 \text{ GeV}/c^2$ are selected for further analysis. Backgrounds containing π^0 are suppressed by rejecting events with $|M(\gamma\gamma) - m_{\pi^0}| < 0.02 \text{ GeV}/c^2$. The invariant mass distribution of $\eta\pi^+\pi^-$ is shown in Fig. 1(b).

IV. MEASUREMENT OF $\chi_{cJ} \rightarrow \eta\eta\eta'$

A. Background estimation

Potential backgrounds are studied using the inclusive MC samples of $\psi(3686)$ decays. The backgrounds are found to fall into three categories: non- χ_{cJ} , non- η' , and processes involving both η' and χ_{cJ} . Non- χ_{cJ} backgrounds are modeled by a polynomial function when fitting the invariant mass distributions of $\eta\eta\eta'$. Non- η' backgrounds are estimated using the η' mass sidebands in the data. The sideband regions for η' are defined as $[0.925, 0.935]$ and $[0.98, 0.99] \text{ GeV}/c^2$. The η' signal shape is determined from the shape of the signal MC sample, and the η' sideband shape is described by a linear function. The backgrounds containing both χ_{cJ} and η' are peaking backgrounds. For peaking backgrounds, the branching fractions from PDG and the efficiency obtained from background MC samples are used to estimate the number of events, which are then fixed in the

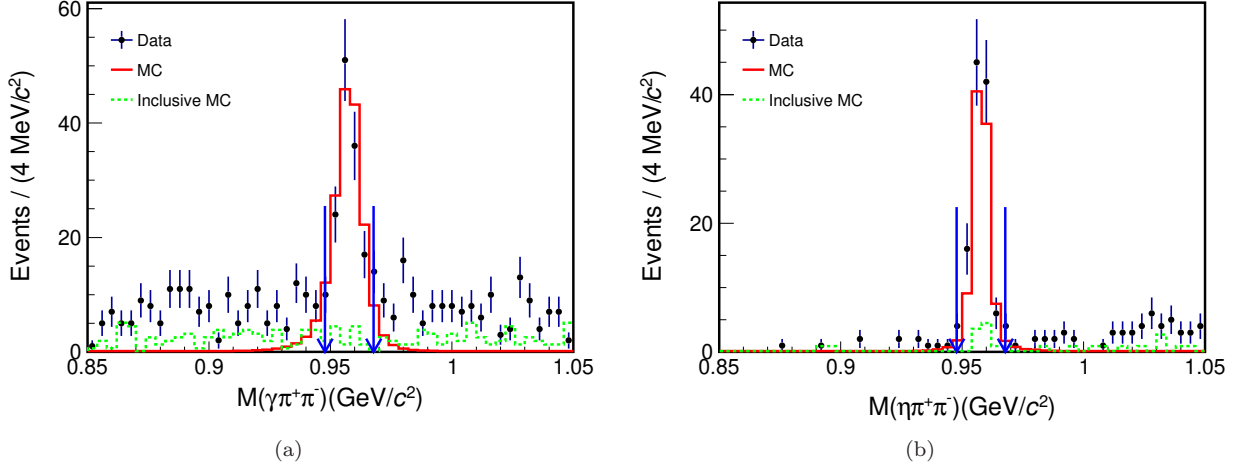


Figure 1. Invariant mass distributions of (a) $\eta' \rightarrow \gamma\pi^+\pi^-$ and (b) $\eta' \rightarrow \eta\pi^+\pi^-$ within all χ_{cJ} range (3.34–3.64 GeV/c^2). The black points with error bars are data, the red solid histograms are the signal MC and the green dashed histograms are the inclusive MC. The events between the blue arrows are the selected signal events.

fit. The peaking backgrounds for the decay mode $\eta' \rightarrow \gamma\pi^+\pi^-$ primarily arise from $\chi_{c1} \rightarrow \gamma J/\psi, J/\psi \rightarrow \gamma\eta\eta'$ and $\chi_{c2} \rightarrow \gamma J/\psi, J/\psi \rightarrow \gamma\eta\eta'$, with estimated yields (fractions) of 2.25 (1.7%) and 1.14 (0.8%), respectively. Similarly, the peaking backgrounds for the decay mode $\eta' \rightarrow \eta\pi^+\pi^-$ are mainly from $\chi_{c1} \rightarrow \gamma J/\psi, J/\psi \rightarrow \gamma\eta\eta'$, $\chi_{c2} \rightarrow \gamma J/\psi, J/\psi \rightarrow \gamma\eta\eta'$ and $\chi_{c0} \rightarrow \eta'\eta'$, with estimated yields (fractions) of 1.97 (1.7%), 0.82 (0.7%) and 1.25 (1.1%), respectively. The backgrounds with a fraction of no more than 1.0% are neglected.

B. Signal extraction

The $\eta\eta\eta'$ invariant mass distributions for the $\eta' \rightarrow \gamma\pi^+\pi^-$ and $\eta' \rightarrow \eta\pi^+\pi^-$ modes are shown in Fig. 2. We perform a simultaneous unbinned maximum likelihood fit to the $\eta\eta\eta'$ distributions in the range of [3.34, 3.64] GeV/c^2 . The χ_{c0} , χ_{c1} , and χ_{c2} signals are modeled using the shape of MC samples convolved with a Gaussian function to account for the mass resolution and describe the difference between data and MC simulation. Parameters of the Gaussian function are treated as free parameters. The peaking backgrounds are normalized and fixed based on the MC simulations. The non- η' background events are described by the η' mass sidebands and are fixed in the fit. The remaining background is described by a linear function with free parameters. In the simultaneous fit, the fitted yields of $\mathcal{N}_{\text{sig},1}$ and $\mathcal{N}_{\text{sig},2}$ are constrained to the common number of produced $\chi_{cJ} \rightarrow \eta\eta\eta'$ events $\mathcal{N}_{\text{sig}}^{\chi_{cJ}}$, which is defined as:

$$\begin{aligned} \mathcal{N}_{\text{sig}}^{\chi_{cJ}} &= \frac{\mathcal{N}_{\text{sig},1}}{\epsilon_1 \cdot \mathcal{B}(\eta' \rightarrow \gamma\pi^+\pi^-) \cdot \mathcal{B}(\eta \rightarrow \gamma\gamma)^2} \\ &= \frac{\mathcal{N}_{\text{sig},2}}{\epsilon_2 \cdot \mathcal{B}(\eta' \rightarrow \eta\pi^+\pi^-) \cdot \mathcal{B}(\eta \rightarrow \gamma\gamma)^3}, \end{aligned} \quad (1)$$

where indices 1 and 2 represent $\eta' \rightarrow \gamma\pi^+\pi^-$ and $\eta' \rightarrow \eta\pi^+\pi^-$, respectively. $\mathcal{N}_{\text{sig},1}$ and $\mathcal{N}_{\text{sig},2}$ are the numbers of observed χ_{cJ} events, ϵ_1 and ϵ_2 are the corresponding detection efficiencies, and the branching fractions are obtained from the PDG [22]. The fit result is shown in Fig. 2.

The branching fractions of $\chi_{cJ} \rightarrow \eta\eta\eta'$ are calculated by

$$\mathcal{B}(\chi_{cJ} \rightarrow \eta\eta\eta') = \frac{\mathcal{N}_{\text{sig}}^{\chi_{cJ}}}{N_{\psi(3686)} \cdot \mathcal{B}(\psi(3686) \rightarrow \gamma\chi_{cJ})}, \quad (2)$$

where $\mathcal{N}_{\text{sig}}^{\chi_{cJ}}$ is defined in Eq. 1, $N_{\psi(3686)}$ is the number of $\psi(3686)$ events and $\mathcal{B}(\psi(3686) \rightarrow \gamma\chi_{cJ})$ is the branching fraction of $\psi(3686) \rightarrow \gamma\chi_{cJ}$ obtained from PDG [22]. Since no clear signal for χ_{c0} exists, a Bayesian method is used to obtain the upper limit of the signal yield at 90% confidence level (CL). To determine the upper limit of the signal yield, the distribution of normalized likelihood values for a series of expected signal yields is taken as the probability density function (PDF). In obtaining the distribution of likelihood values, the signals of χ_{c1} and χ_{c2} are described by the MC shape function convolved with a Gaussian function, and their parameters are free. The upper limit of the signal yields at the 90% CL, denoted as N^{UL} , is defined as the number of events where 90% of the PDF area lies above zero. These results of branching fractions are listed in Table I.

C. Systematic uncertainties

The systematic uncertainties of $\mathcal{B}(\chi_{cJ} \rightarrow \eta\eta\eta')$ are summarized below.

1. Number of $\psi(3686)$ events. The number of $\psi(3686)$ events is determined by analyzing inclusive hadronic $\psi(3686)$ decays with an uncertainty of 0.5% [28].

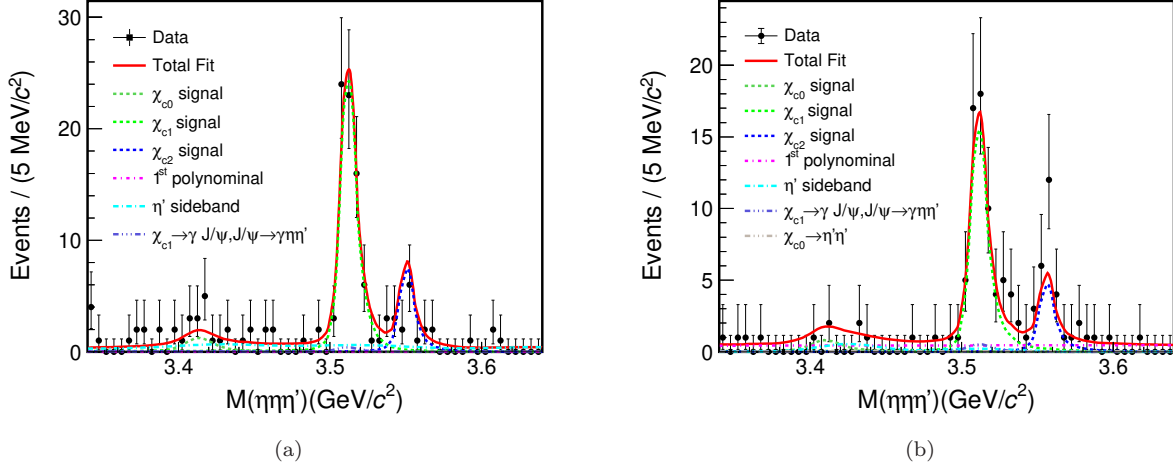


Figure 2. The simultaneous fit results for the invariant mass distributions of $\eta\eta\eta'$ in two decay modes of η' (a) $\eta' \rightarrow \gamma\pi^+\pi^-$ and (b) $\eta' \rightarrow \eta\pi^+\pi^-$. The dots with error bars represent the data, the red solid curves show the fit results, and the dark green, light green, and blue dashed lines represent the signals of χ_{c0} , χ_{c1} and χ_{c2} , while the other dashed lines represent the backgrounds.

Table I. The numbers of the observed χ_{cJ} events ($\mathcal{N}_{\text{sig},1}$ and $\mathcal{N}_{\text{sig},2}$), corresponding detection efficiencies (ϵ_1 and ϵ_2), the number of produced $\chi_{cJ} \rightarrow \eta\eta\eta'$ events ($\mathcal{N}_{\text{sig}}^{\chi_{cJ}}$, which is defined in Eq. 1), branching fractions (\mathcal{B}), and the statistical significance, respectively. Indices 1 and 2 represent $\eta' \rightarrow \gamma\pi^+\pi^-$ and $\eta' \rightarrow \eta\pi^+\pi^-$, respectively. The first and second uncertainties are statistical and systematic, respectively.

χ_{cJ}	$\mathcal{N}_{\text{sig},1}$	$\epsilon_1(\%)$	$\mathcal{N}_{\text{sig},2}$	$\epsilon_2(\%)$	$\mathcal{N}_{\text{sig}}^{\chi_{cJ}}$	$\mathcal{B}(\chi_{cJ} \rightarrow \eta\eta\eta')$	Significance
χ_{c0}	9.3 ± 3.8	5.23 ± 0.02	3.9 ± 1.6	3.86 ± 0.02	3866.0 ± 1568.9	$< 2.64 \times 10^{-5}$	0.1σ
χ_{c1}	97.0 ± 9.3	5.76 ± 0.02	38.5 ± 3.7	4.03 ± 0.02	36768.4 ± 3462.6	$(1.39 \pm 0.13 \pm 0.09) \times 10^{-4}$	15.8σ
χ_{c2}	27.8 ± 5.6	5.32 ± 0.02	11.0 ± 2.2	3.70 ± 0.02	11418.5 ± 2278.4	$(4.42 \pm 0.86 \pm 0.37) \times 10^{-5}$	7.0σ

2. MDC tracking. The data-MC efficiency difference for pion track-finding is studied using a control sample of $J/\psi \rightarrow \rho\pi$ and $J/\psi \rightarrow p\bar{p}\pi^+\pi^-$ [29]. The systematic uncertainty from MDC tracking is 1.0% per charged pion.
3. PID. The pion PID efficiency for data agrees within 1.0% with that of the MC simulation in the pion momentum region, as reported in [29]. Thus, a systematic uncertainty of 2.0% is assigned to PID.
4. Photon reconstruction. For photons detected by the EMC, the detection efficiency is studied using a control sample of $e^+e^- \rightarrow \gamma_{\text{ISR}}\mu^+\mu^-$, where ISR stands for initial state radiation. The systematic uncertainty, defined as the relative difference in efficiencies between data and MC simulation, is observed to be up to 0.5% per photon in both the barrel and end-cap regions.
5. Intermediate decay branching fractions. The uncertainties on the intermediate decay branching fractions are taken from the PDG values [22].
6. Kinematic fit. To investigate the systematic uncertainty associated with the kinematic fit, the track helix parameter correction method is used [30].

The difference in the detection efficiencies with and without the helix correction is taken as the systematic uncertainty.

7. Mass windows of η' and χ_{cJ} . The systematic uncertainty from the requirement on the η' or χ_{cJ} signal region is estimated by smearing the $\gamma\pi^+\pi^-$ ($\eta\pi^+\pi^-$) and $\eta\eta\eta'$ invariant masses in the signal MC sample with a Gaussian function to account for the resolution difference between data and MC simulation. The smearing parameters are determined by fitting the $\gamma\pi^+\pi^-$ ($\eta\pi^+\pi^-$) and $\eta\eta\eta'$ invariant mass distributions in data with the MC shape convolved with a Gaussian function. The difference in the detection efficiency, as determined from the signal MC sample with and without the extra smearing, is taken as the systematic uncertainty.
8. Veto of π^0 . Possible systematic effects due to the veto on π^0 are investigated using the Barlow test [31], by varying the veto criteria between 10 and 50 MeV/c^2 . The uncertainty is assigned as the difference between the nominal result and the result with $|M(\gamma\gamma) - m_{\pi^0}| < 21 \text{ MeV}/c^2$ when 95% of the candidate events are retained. Since there is no

signal in the χ_{c0} process, we set the value of this systematic uncertainty to be the same as that for $\chi_{c1,c2}$.

9. Fit range. The systematic uncertainties due to different fit ranges are examined by enlarging and shrinking the fit range eight times, with a step of 20 MeV/ c^2 . For each case, the deviation between the alternative and nominal fits is defined as $\xi = \frac{|a_1 - a_2|}{\sqrt{|\sigma_1^2 - \sigma_2^2|}}$, where $a_1 \pm \sigma_1$ and $a_2 \pm \sigma_2$ are the nominal fit results and alternative fit results, respectively. If ξ is less than 2.0, the associated systematic uncertainty is negligible according to the Barlow test [31]. The largest difference is assigned as the systematic uncertainty.
10. Non-peaking background shape. The systematic uncertainty due to the background shape is estimated by replacing the linear function with a second-order polynomial in the fit. The maximum difference in the signal yields compared to the nominal value is taken as the uncertainty.
11. η' sideband. The uncertainties from the η' sideband region are estimated by changing sideband regions to [0.93, 0.94] and [0.975, 0.985] GeV/ c^2 . The maximum difference in signal yields compared to the nominal value is taken as the uncertainty.
12. Peaking background. The uncertainties from the peaking background are estimated by changing the fixed number of peaking background events, which is calculated through the propagation of branching fraction errors. The fixed branching fraction values of peaking background are calculated by adding or subtracting 1σ from the nominal value of these processes. The maximum difference in signal yields compared to the nominal value is taken as the uncertainty.

For the two η' decay modes, some systematic uncertainties are common, while others are independent. The combination of common and independent systematic uncertainties for these two decay modes are calculated using the weighted least squares method [32].

For the calculation of $\mathcal{B}(\chi_{c1,c2} \rightarrow \eta\eta\eta')$, the sources of systematic uncertainties are listed in Table II. Their branching fractions are determined to be $\mathcal{B}(\chi_{c1} \rightarrow \eta\eta\eta') = (1.39 \pm 0.13(\text{stat.}) \pm 0.09(\text{sys.})) \times 10^{-4}$ and $\mathcal{B}(\chi_{c2} \rightarrow \eta\eta\eta') = (4.42 \pm 0.86(\text{stat.}) \pm 0.37(\text{sys.})) \times 10^{-5}$, respectively. It is noted that $\mathcal{B}(\chi_{c1} \rightarrow \pi^+\pi^-\eta') = (2.2 \pm 0.4) \times 10^{-3}$ and $\mathcal{B}(\chi_{c2} \rightarrow \pi^+\pi^-\eta') = (5.1 \pm 1.9) \times 10^{-4}$ [22]. In comparison, the branching fractions of $\chi_{c1,c2} \rightarrow \eta\eta\eta'$ obtained in this analysis are an order of magnitude smaller than those of $\chi_{c1,c2} \rightarrow \pi^+\pi^-\eta'$.

The systematic uncertainties of $\mathcal{B}(\chi_{c0} \rightarrow \eta\eta\eta')$ are divided into two categories. The first category includes the multiplicative systematic uncertainties related to event selection, which are summarized in Table III. The second

Table II. Summary of relative systematic uncertainties for $\mathcal{B}(\chi_{c1,c2} \rightarrow \eta\eta\eta')$ (in %). The symbol “-” denotes unapplicable items.

Source	Independent systematic uncertainties			
	χ_{c1}	χ_{c2}	$\gamma\pi^+\pi^-\eta\pi^+\pi^-$	$\gamma\pi^+\pi^-\eta\pi^+\pi^-$
Another photon reconstruction	-	0.5	-	0.5
$\mathcal{B}(\eta \rightarrow \gamma\gamma)$	-	0.5	-	0.5
$\mathcal{B}(\eta' \rightarrow \gamma(\eta)\pi^+\pi^-)$	1.4	1.2	1.4	1.2
Kinematic fit	0.7	0.1	0.9	0.2
η' mass window	0.1	0.1	0.1	0
Total	1.6	1.4	1.7	1.4
Common systematic uncertainties				
Source	χ_{c1}	χ_{c2}		
$N_\psi(3686)$		0.5		
Two pion tracking		2.0		
PID		2.0		
Six photon reconstruction		3.0		
$\mathcal{B}(\eta \rightarrow \gamma\gamma)$		1.0		
$\mathcal{B}(\psi(3686) \rightarrow \gamma\chi_{c1})$	2.8	2.5		
Veto π^0	1.5	1.5		
Fit range	1.4	2.5		
Background shape	2.2	0.2		
η' sideband	2.9	3.4		
Peaking background	0.7	4.8		
Total	6.6	8.3		
Combined systematic uncertainties	6.7	8.4		

category consists of the additive systematic uncertainties related to the fit, such as the fit range, background shape, η' sideband and peaking background. Perform each alternative fit and set the maximum value as the upper limit.

Table III. Summary of relative multiplicative systematic uncertainties for the upper limit of $\mathcal{B}(\chi_{c0} \rightarrow \eta\eta\eta')$ (in %).

Source	Independent multiplicative systematic uncertainties			
	χ_{c0}	χ_{c0}	$\gamma\pi^+\pi^-\eta\pi^+\pi^-$	$\gamma\pi^+\pi^-\eta\pi^+\pi^-$
Another photon reconstruction	-	0.5	-	0.5
$\mathcal{B}(\eta \rightarrow \gamma\gamma)$	-	0.5	-	0.5
$\mathcal{B}(\eta' \rightarrow \gamma(\eta)\pi^+\pi^-)$	1.4	1.2	-	-
Kinematic fit	1.0	0.2	-	-
η' mass window	0.1	0.1	-	-
Total	1.7	1.4	-	-
Common multiplicative systematic uncertainties				
Source	χ_{c0}			
$N_\psi(3686)$	0.5			
Two pion tracking	2.0			
PID	2.0			
Six photon reconstruction	3.0			
$\mathcal{B}(\eta \rightarrow \gamma\gamma)$	1.0			
$\mathcal{B}(\psi(3686) \rightarrow \gamma\chi_{c0})$	2.4			
Veto π^0	1.5			
Total	5.1			
Combined multiplicative uncertainties	5.2			

To obtain a conservative estimate of the upper limit of $\mathcal{B}(\chi_{c0} \rightarrow \eta\eta\eta')$, the likelihood distribution is smeared by a Gaussian function with a mean of zero and a width of

σ_ϵ ,

$$L'(n') \propto \int_0^1 L(n \frac{\epsilon}{\epsilon_0}) \exp\left[-\frac{(\epsilon - \epsilon_0)^2}{2\sigma_\epsilon^2}\right] d\epsilon, \quad (3)$$

where $L(n)$ is the likelihood distribution as a Gaussian function of the yield n , ϵ_0 is the detection efficiency calculated by $\frac{\sum_i B_i \epsilon_i}{\sum_i B_i}$, and σ_ϵ is the multiplicative systematic uncertainty. $L'(n')$ is the smeared likelihood distribution. The upper limit of $\mathcal{B}(\chi_{c0} \rightarrow \eta\eta\eta')$ is estimated to be 2.64×10^{-5} .

V. SEARCH FOR $\chi_{c1} \rightarrow \eta_1(1855)\eta, \eta_1(1855) \rightarrow \eta\eta'$

To search for the $\chi_{c1} \rightarrow \eta_1(1855)\eta, \eta_1(1855) \rightarrow \eta\eta'$ process, the $\eta\eta\eta'$ invariant mass of the χ_{c1} candidates must distribute within [3.50, 3.53] GeV/c^2 . After the event selections, the invariant mass spectra and Dalitz plots of data are shown in Fig. 3.

A. Background estimation

Potential backgrounds are studied using the inclusive MC samples of $\psi(3686)$ decays. The results show that the backgrounds can be divided into two categories: non- η' processes and those containing η' . Non- η' backgrounds are estimated using the η' mass sidebands in the data. The sideband regions of η' are defined as [0.925, 0.935] and [0.98, 0.99] GeV/c^2 . The normalization factors for events in the two sideband regions are obtained by fitting the invariant mass distributions of $\gamma\pi^+\pi^-$ and $\eta\pi^+\pi^-$ in the data. The η' signal shapes are determined from the shapes of signal MC samples, while the η' sideband shapes are described using linear functions. The backgrounds containing η' are peaking backgrounds. For this type of background, the branching fractions from the PDG and the efficiency obtained from background MC samples are used to estimate the normalized number of events, which is then fixed in the fit. The peaking backgrounds for the decay mode $\eta' \rightarrow \gamma\pi^+\pi^-$ mainly come from $\chi_{c1} \rightarrow \eta J/\psi, J/\psi \rightarrow \gamma\eta\eta'$ and $\chi_{c1} \rightarrow \gamma J/\psi, J/\psi \rightarrow \gamma\eta\eta'$, with estimated yields (fractions) of 0.2 (0.2%) and 1.9 (2.6%), respectively. Similarly, the peaking backgrounds for the decay mode $\eta' \rightarrow \eta\pi^+\pi^-$ mainly come from $\chi_{c1} \rightarrow \gamma J/\psi, J/\psi \rightarrow \gamma\eta\eta'$ and $\chi_{c0} \rightarrow \eta'\eta'$, with estimated yields (fractions) of 1.5 (2.6%) and 0.2 (0.3%), respectively. The background with a fraction of no more than 1.0% is neglected.

B. PWA method

For the two η' decay modes, there are 73 and 59 events left in the data, which are used to perform the PWA fit. The four-momenta of $\psi(3686)$, γ , η , η and η' after the

5C kinematic fit are used in the PWA. The decay amplitude is constructed using the helicity amplitude formalism, and the full procedure is implemented based on the open-source framework TF-PWA[33]. To construct the full decay amplitude of $\psi(3686) \rightarrow \gamma\eta\eta\eta'$, the helicity formalism is used in conjunction with the isobar model, where the four-body decay is described as a two-step sequential quasi-two-body decay. For each two-body decay $A \rightarrow B + C$, the helicity amplitude can be written as:

$$A_{\lambda_A, \lambda_B, \lambda_C}^{A \rightarrow B+C} = F_{\lambda_B \lambda_C} D_{\lambda_A, \lambda_{B-C}}^{j_A*}(\phi, \theta, 0), \quad (4)$$

where $D_{\lambda_A, \lambda_{B-C}}^{j_A*}(\phi, \theta, 0)$ represents the Wigner D-function, ϕ and θ are the helicity angles, and $F_{\lambda_B \lambda_C}$ is the helicity coupling amplitude, which can be described using the LS coupling formula,

$$F_{\lambda_B \lambda_C} = \sum_{ls} g_{ls} \sqrt{\frac{2l+1}{2J+1}} \langle j_B \lambda_B; j_C - \lambda_C | s\delta \rangle \langle l0; s\delta | J\delta \rangle q^l B'_l(q, q_0, d), \quad (5)$$

where g_{ls} represents the fitting parameter, $\lambda_{B(C)}$ is the helicity, q and q_0 are the momentum of the invariant mass and the mass of the resonance state in the rest frame, and $B'_l(q, q_0, d)$ is the Blatt-Weisskopf barrier factor.

The full amplitude for the complete decay chain $A \rightarrow R_1 + B, R_1 \rightarrow R_2 + C, R_2 \rightarrow D + E$ is constructed as the product of each two-body decay amplitude and the resonant propagator $R_1(\chi_{c1})$ and R_2 . The amplitude is written as Eq. 6, where A, B, C, D, E are $\psi(3686), \gamma, \eta, \eta$ and η' , respectively. The propagator R uses the relativistic Breit-Wigner formula with constant width: $BW(s) = \frac{1}{M^2 - s - iM\Gamma}$, where M and Γ are the mass and width of resonances, and \sqrt{s} is the invariant mass of $\eta\eta'$ or $\eta\eta$. Backgrounds in the PWA are estimated by using normalized η' sidebands and the fixed MC shape in the processes of peaking backgrounds.

The construction of the probability density function, the calculation of the fit fraction, and the corresponding statistical uncertainty for each component follow Ref.[34]. The combined branching fraction is obtained according to Eq. 7.

C. PWA result

From the mass spectrum, no obvious structure is observed in the $\eta\eta$ mass spectrum, while a structure is seen near the threshold in the mass spectrum of $\eta\eta'$. Therefore, the S-wave nonresonant (NR) component and $f_0(1500)$ in the $\eta\eta$ mass spectrum, as well as the S-wave NR component, $f_0(1500)$, and $\eta_1(1855)$ in the $\eta\eta'$ mass spectrum, are considered. The mass and width of $\eta_1(1855)$ are fixed at $1855 \text{ MeV}/c^2$ and $188 \text{ MeV}/c^2$ as given in the Ref. [9, 10]. The statistical significance for each component is determined by examining the change in negative log-likelihood values when this resonance is

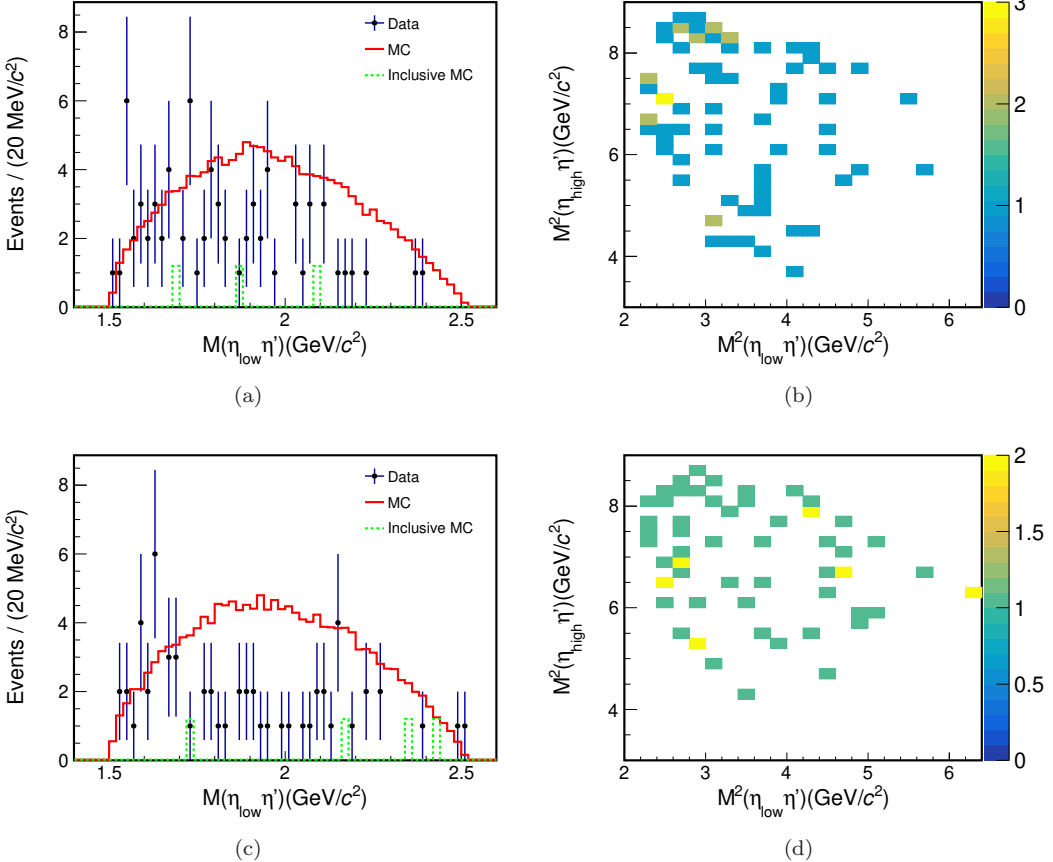


Figure 3. Invariant mass distributions and Dalitz plots for (a)(b) $\chi_{c1} \rightarrow \eta\eta\eta', \eta' \rightarrow \gamma\pi^+\pi^-$, (c)(d) $\chi_{c1} \rightarrow \eta\eta\eta', \eta' \rightarrow \eta\pi^+\pi^-$. The dots with error bars are data, the red solid histograms are the signal MC, and the green dashed histograms are inclusive MC. η_{low} denotes the low energy η .

$$\begin{aligned}
& A_{\lambda_A, \lambda'_B, \lambda'_C, \lambda'_D, \lambda'_E}^{R_1, R_2} = F_{\lambda_{R_1} \lambda_B} D_{\lambda_A, \lambda_{R_1} - \lambda_B}^{j_{A*}}(\varphi_1, \theta_1, 0) R_1(\mathbf{M}) F_{\lambda_{R_2} \lambda_C} D_{\lambda_{R_1}, \lambda_{R_2} - \lambda_C}^{j_{R_1*}}(\varphi_2, \theta_2, 0) R_2(\mathbf{M}) F_{\lambda_D \lambda_E} D_{\lambda_{R_2}, \lambda_D - \lambda_E}^{j_{R_2*}}(\varphi_3, \theta_3, 0) \\
& D_{\lambda_B, \lambda_{B'}}^{j_{B*}}(\alpha_B, \beta_B, \gamma_B) D_{\lambda_C, \lambda_{C'}}^{j_{C*}}(\alpha_C, \beta_{C'}, \gamma_C) D_{\lambda_D, \lambda_{D'}}^{j_{D*}}(\alpha_D, \beta_D, \gamma_D) D_{\lambda_E, \lambda_{E'}}^{j_{E*}}(\alpha_E, \beta_E, \gamma_E).
\end{aligned} \tag{6}$$

included or excluded in the fits. The probability is calculated under the χ^2 distribution hypothesis considering the change in the number of degrees of freedom. Resonance with a statistical significance greater than 5σ is included in the final set of amplitudes.

The results of the PWA show that the structure in the $\eta\eta'$ mass spectrum is dominated by $f_0(1500)$ with the statistical significance of 6.5σ , while the structure of $\eta\eta$ is mainly described by the 0^{++} NR component. Fig. 4 displays the projection plots of the fitting results of the PWA basic solution. The statistical significance of an additional $\eta_1(1855)$ resonance is determined to be 0.7σ . An upper limit of branching fraction $\mathcal{B}(\chi_{c1} \rightarrow \eta_1(1855)\eta) \cdot \mathcal{B}(\eta_1(1855) \rightarrow \eta\eta')$ is set. The systematic uncertainties will be described below.

D. Systematic uncertainties

The systematic uncertainties are divided into two categories. The first category consists of the multiplicative systematic uncertainties related to event selection, summarized in Table IV. The second category arises from the PWA, with each alternative fit discussed below.

1. Uncertainties from η' sideband background and peaking background are treated as before.
2. Uncertainty from additional resonances. To investigate the impact of other possible components on the PWA results, 0^{++} NR component is added to the mass spectrum of $\eta\eta'$, or $f_0(1500)$ is added to the mass spectrum of $\eta\eta$.
3. Uncertainty from resonance parameters. In the

$$\begin{aligned}
& \mathcal{B}(\chi_{c1} \rightarrow X\eta(\eta')) \cdot \mathcal{B}(X \rightarrow \eta\eta'(\eta\eta)) \\
&= \frac{N_{X_a} + N_{X_b}}{N_{\psi(3686)} \cdot \mathcal{B}(\psi(3686) \rightarrow \gamma\chi_{c1}) \cdot \mathcal{B}^2(\eta \rightarrow \gamma\gamma) \cdot (\epsilon_{X_a} \cdot \mathcal{B}(\eta' \rightarrow \gamma\pi) + \epsilon_{X_b} \cdot \mathcal{B}(\eta' \rightarrow \eta\pi\pi)) \cdot \mathcal{B}(\eta \rightarrow \gamma\gamma)}. \tag{7}
\end{aligned}$$

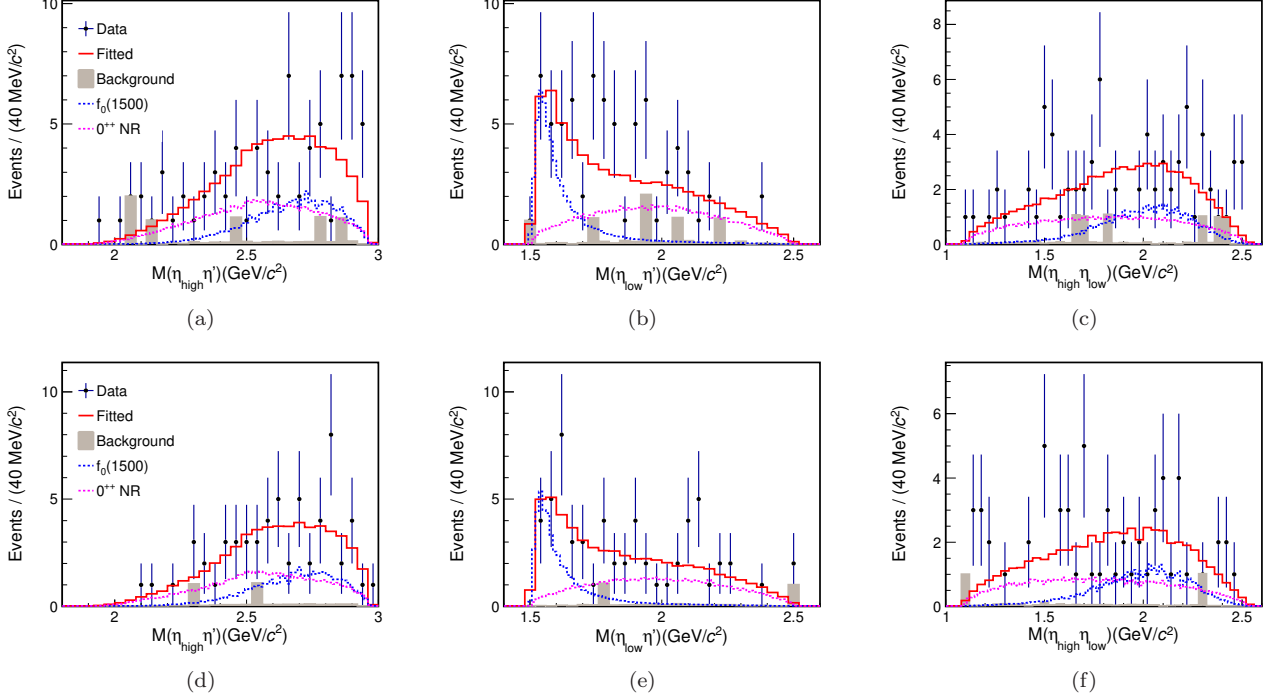


Figure 4. Data (black points with error bars) and the PWA fit projections (lines) for (a)(b)(c) $\chi_{c1} \rightarrow \eta\eta\eta'$, $\eta' \rightarrow \gamma\pi^+\pi^-$ and (d)(e)(f) $\chi_{c1} \rightarrow \eta\eta\eta'$, $\eta' \rightarrow \eta\pi^+\pi^-$. The invariant mass distributions of (a)(d) $\eta_{\text{high}}\eta'$, (b)(e) $\eta_{\text{low}}\eta'$ and (c)(f) $\eta_{\text{high}}\eta_{\text{low}}$. The red solid lines are the total fit projections from the PWA, the gray shadows are the background (from η' sideband and peaking background), the blue dashed lines are the $f_0(1500)$ and the pink dashed lines are the 0^{++} NR components.

baseline fit, the resonance parameters of the $\eta_1(1855)$ are fixed to PDG values [22]. An alternative fit is performed where resonance parameters are allowed to vary within one standard deviation of the PDG values, and the changes in the results are taken as systematic uncertainties.

Table IV. Summary of relative multiplicative systematic uncertainties for $\mathcal{B}(\chi_{c1} \rightarrow \eta\eta_1(1855), \eta_1(1855) \rightarrow \eta\eta')$ (in %).

Independent multiplicative systematic uncertainties		
Source	$\gamma\pi^+\pi^-$	$\eta\pi^+\pi^-$
Another photon reconstruction	-	0.5
$\mathcal{B}(\eta \rightarrow \gamma\gamma)$	-	0.5
$\mathcal{B}(\eta' \rightarrow \gamma(\eta)\pi^+\pi^-)$	1.4	1.2
Kinematic fit	0.8	0.1
η' mass window	0.1	0
χ_{c1} mass window	0.1	0
Total	1.6	1.4
Common multiplicative systematic uncertainties		
Source	$\gamma\pi^+\pi^-$	$\eta\pi^+\pi^-$
$N_{\psi(3686)}$	0.5	
Two pion tracking	2.0	
PID	2.0	
Six photon reconstruction	3.0	
$\mathcal{B}(\eta \rightarrow \gamma\gamma)$	1.0	
$\mathcal{B}(\psi(3686) \rightarrow \gamma\chi_{c1})$	2.8	
Veto π^0	1.5	
Total	5.3	
Combined multiplicative uncertainties	5.4	

For the systematic uncertainties associated with the PWA, the maximum value of the upper limit is chosen for each case. Considering multiplicative systematic uncertainties associated with event selections, the likelihood distribution is smeared using a Gaussian function with a mean of zero and a width of σ_ϵ , as Eq. 3, where $L(n)$ is a Gaussian distribution with mean and error from the PWA branching fraction, ϵ_0 is the detection efficiency obtained by PWA, and σ_ϵ is the combined multiplicative systematic uncertainty. $L'(n')$ is the smeared likelihood distribution. Taking the smearing distribution with an area of 90% as the upper limit, the result is $\mathcal{B}(\chi_{c1} \rightarrow \eta_1(1855)\eta) \cdot \mathcal{B}(\eta_1(1855) \rightarrow \eta\eta') < 9.79 \times 10^{-5}$.

VI. SUMMARY

In summary, a study of the decays $\chi_{cJ} \rightarrow \eta\eta\eta'$ and a PWA of $\chi_{c1} \rightarrow \eta\eta\eta'$ are performed based on $2.7 \times 10^9 \psi(3686)$ events collected with the BESIII detector. The decay modes $\chi_{c1,c2} \rightarrow \eta\eta\eta'$ are observed for the first time, and their corresponding branching fractions are determined to be $\mathcal{B}(\chi_{c1} \rightarrow \eta\eta\eta') = (1.39 \pm 0.13(\text{stat.}) \pm 0.09(\text{sys.})) \times 10^{-4}$ and $\mathcal{B}(\chi_{c2} \rightarrow \eta\eta\eta') = (4.42 \pm 0.86(\text{stat.}) \pm 0.37(\text{sys.})) \times 10^{-5}$, which are one order of magnitude lower than those of $\chi_{c1,c2} \rightarrow \pi^+\pi^-\eta'$ in PDG [22]. An upper limit of 2.64×10^{-5} at 90% CL is set for the decay $\chi_{c0} \rightarrow \eta\eta\eta'$. Subsequently, a PWA of the decay $\chi_{c1} \rightarrow \eta\eta\eta'$ is performed to search for the 1^{-+} exotic state $\eta_1(1855)$. The PWA result indicates that the structure in the $\eta\eta'$ mass spectrum is mainly attributed to $f_0(1500)$, while in the $\eta\eta$ mass spectrum, it is primarily the 0^{++} NR component. No significant $\eta_1(1855)$ is observed. The upper limit of $\mathcal{B}(\chi_{c1} \rightarrow \eta_1(1855)\eta) \cdot \mathcal{B}(\eta_1(1855) \rightarrow \eta\eta') < 9.79 \times 10^{-5}$ is obtained at 90% CL. In further research, the $\eta\eta'$ decay mode with an increased dataset and more decay modes will be explored to study $\eta_1(1855)$.

VII. ACKNOWLEDGMENT

The BESIII Collaboration thanks the staff of BEPCII (<https://cstr.cn/31109.02.BEPC>) and the IHEP computing center for their strong support. This work is supported in part by National Key R&D Program of China under Contracts Nos. 2023YFA1606000, 2023YFA1606704; National Natural Science Foundation of China (NSFC) under Contracts Nos. 11635010, 11935015, 11935016, 11935018, 12025502, 12035009, 12035013, 12061131003, 12192260, 12192261, 12192262, 12192263, 12192264, 12192265, 12221005, 12225509, 12235017, 12361141819; the Chinese Academy of Sciences (CAS) Large-Scale Scientific Facility Program; CAS under Contract No. YSBR-101; 100 Talents Program of CAS; The Institute of Nuclear and Particle Physics (INPAC) and Shanghai Key Laboratory for Particle Physics and Cosmology; Agencia Nacional de Investigación y Desarrollo de Chile (ANID), Chile under Contract No. ANID PIA/APOYO AFB230003; German Research Foundation DFG under Contract No. FOR5327; Istituto Nazionale di Fisica Nucleare, Italy; Knut and Alice Wallenberg Foundation under Contracts Nos. 2021.0174, 2021.0299; Ministry of Development of Turkey under Contract No. DPT2006K-120470; National Research Foundation of Korea under Contract No. NRF-2022R1A2C1092335; National Science and Technology fund of Mongolia; National Science Research and Innovation Fund (NSRF) via the Program Management Unit for Human Resources & Institutional Development, Research and Innovation of Thailand under Contract No. B50G670107; Polish National Science Centre under Contract No. 2024/53/B/ST2/00975; Swedish Research Council under Contract No. 2019.04595; U. S. Department of Energy under Contract No. DE-FG02-05ER41374.

- [1] J. J. Dudek, R. G. Edwards, P. Guo, and C. E. Thomas (Hadron Spectrum), *Phys. Rev. D* **88**, 094505 (2013), [arXiv:1309.2608 \[hep-lat\]](https://arxiv.org/abs/1309.2608).
- [2] F. Chen, X. Jiang, Y. Chen, M. Gong, Z. Liu, C. Shi, and W. Sun, *Phys. Rev. D* **107**, 054511 (2023), [arXiv:2207.04694 \[hep-lat\]](https://arxiv.org/abs/2207.04694).
- [3] J. Liang, S. Chen, Y. Chen, C. Shi, and W. Sun, *Sci. China Phys. Mech. Astron.* **68**, 251011 (2025), [arXiv:2409.14410 \[hep-lat\]](https://arxiv.org/abs/2409.14410).
- [4] C. A. Meyer and E. S. Swanson, *Prog. Part. Nucl. Phys.* **82**, 21 (2015), [arXiv:1502.07276 \[hep-ph\]](https://arxiv.org/abs/1502.07276).
- [5] P.-Z. Huang, H.-X. Chen, and S.-L. Zhu, *Phys. Rev. D* **83**, 014021 (2011), [arXiv:1010.2293 \[hep-ph\]](https://arxiv.org/abs/1010.2293).
- [6] H.-X. Chen, Z.-X. Cai, P.-Z. Huang, and S.-L. Zhu, *Phys. Rev. D* **83**, 014006 (2011), [arXiv:1010.3974 \[hep-ph\]](https://arxiv.org/abs/1010.3974).
- [7] W. I. Eshraim, C. S. Fischer, F. Giacosa, and D. Parganlija, *Eur. Phys. J. Plus* **135**, 945 (2020), [arXiv:2001.06106 \[hep-ph\]](https://arxiv.org/abs/2001.06106).
- [8] G. S. Adams *et al.* (CLEO), *Phys. Rev. D* **84**, 112009 (2011), [arXiv:1109.5843 \[hep-ex\]](https://arxiv.org/abs/1109.5843).
- [9] M. Ablikim *et al.* (BESIII), *Phys. Rev. Lett.* **129**, 192002 (2022), [Erratum: *Phys. Rev. Lett.* 130, 159901 (2023)], [arXiv:2202.00621 \[hep-ex\]](https://arxiv.org/abs/2202.00621).
- [10] M. Ablikim *et al.* (BESIII), *Phys. Rev. D* **106**, 072012 (2022), [Erratum: *Phys. Rev. D* 107, 079901 (2023)], [arXiv:2202.00623 \[hep-ex\]](https://arxiv.org/abs/2202.00623).
- [11] M. Ablikim *et al.* (BESIII), *Nucl. Instrum. Meth. A* **614**, 345 (2010), [arXiv:0911.4960 \[physics.ins-det\]](https://arxiv.org/abs/0911.4960).
- [12] C. Yu *et al.*, in *7th International Particle Accelerator Conference* (2016) p. TUYA01.
- [13] M. Ablikim *et al.* (BESIII), *Chin. Phys. C* **44**, 040001 (2020), [arXiv:1912.05983 \[hep-ex\]](https://arxiv.org/abs/1912.05983).
- [14] X. Li *et al.*, *Radiat. Detect. Technol. Methods* **1**, 13 (2017).
- [15] Y.-X. Guo *et al.*, *Radiat. Detect. Technol. Methods* **1**, 15 (2017).

- [16] P. Cao *et al.*, *Nucl. Instrum. Meth. A* **953**, 163053 (2020).
- [17] S. Agostinelli *et al.* (GEANT4), *Nucl. Instrum. Meth. A* **506**, 250 (2003).
- [18] S. Jadach, B. F. L. Ward, and Z. Was, *Comput. Phys. Commun.* **130**, 260 (2000), [arXiv:hep-ph/9912214](https://arxiv.org/abs/hep-ph/9912214).
- [19] S. Jadach, B. F. L. Ward, and Z. Was, *Phys. Rev. D* **63**, 113009 (2001), [arXiv:hep-ph/0006359](https://arxiv.org/abs/hep-ph/0006359).
- [20] D. J. Lange, *Nucl. Instrum. Meth. A* **462**, 152 (2001).
- [21] R.-G. Ping, *Chin. Phys. C* **32**, 599 (2008).
- [22] S. Navas *et al.* (Particle Data Group), *Phys. Rev. D* **110**, 030001 (2024).
- [23] J. C. Chen, G. S. Huang, X. R. Qi, D. H. Zhang, and Y. S. Zhu, *Phys. Rev. D* **62**, 034003 (2000).
- [24] R.-L. Yang, R.-G. Ping, and H. Chen, *Chin. Phys. Lett.* **31**, 061301 (2014).
- [25] E. Barberio, B. van Eijk, and Z. Was, *Comput. Phys. Commun.* **66**, 115 (1991).
- [26] M. Ablikim *et al.* (BESIII), *Phys. Rev. Lett.* **120**, 242003 (2018), [arXiv:1712.01525](https://arxiv.org/abs/1712.01525) [hep-ex].
- [27] M. Ablikim *et al.* (BESIII), *Phys. Rev. D* **97**, 012003 (2018), [arXiv:1709.04627](https://arxiv.org/abs/1709.04627) [hep-ex].
- [28] M. Ablikim *et al.* (BESIII), *Chin. Phys. C* **48**, 093001 (2024), [arXiv:2403.06766](https://arxiv.org/abs/2403.06766) [hep-ex].
- [29] M. Ablikim *et al.* (BESIII), *Phys. Rev. Lett.* **112**, 022001 (2014), [arXiv:1310.1163](https://arxiv.org/abs/1310.1163) [hep-ex].
- [30] M. Ablikim *et al.* (BESIII), *Phys. Rev. D* **87**, 012002 (2013), [arXiv:1208.4805](https://arxiv.org/abs/1208.4805) [hep-ex].
- [31] R. Barlow, in *Conference on Advanced Statistical Techniques in Particle Physics* (2002) pp. 134–144, [arXiv:hep-ex/0207026](https://arxiv.org/abs/hep-ex/0207026).
- [32] G. D'Agostini, *Nucl. Instrum. Meth. A* **346**, 306 (1994).
- [33] Y. Jiang, *Nuovo Cim. C* **47**, 203 (2024).
- [34] E. Oset, A. Ramos, and C. Bennhold, *Phys. Lett. B* **527**, 99 (2002), [Erratum: *Phys. Lett. B* 530, 260–260 (2002)], [arXiv:nucl-th/0109006](https://arxiv.org/abs/nucl-th/0109006).